Journal of Materials Chemistry C

Accepted Manuscript

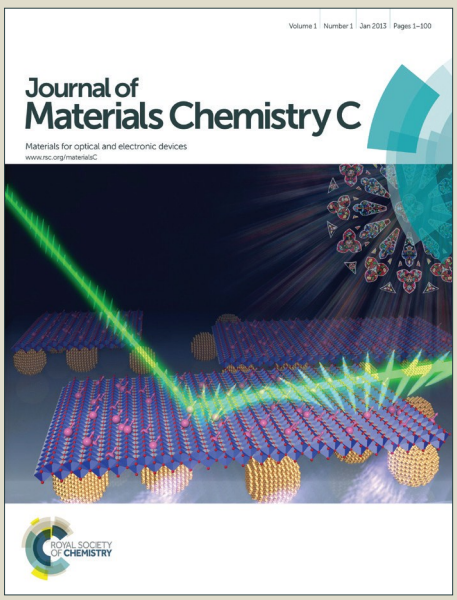

ROYAL SOCIETY OF CHEMISTRY

www.rsc.org/materialsC

Journal of Materials Chemistry C

RSCPublishing

COMMUNICATION

Mixed Self-Assembled Monolayer Gate Dielectrics For Low-Voltage Solution-Processed Polymer Field-Effect Transistors

Cite this: DOI: 10.1039/x0xx00000x

Received 00th September 2014,
Accepted 00th September 2014

DOI: 10.1039/x0xx00000x

www.rsc.org/

T. V. A. G. de Oliveira[a], A. Eleta[a], L. E. Hueso[a,b], and A. M. Bittner[a,b,*]

Ultrathin hybrid gate dielectrics based on aluminum oxide (AlOx) and a mixed-type phosphonic-acid self-assembled monolayers (PA-SAM) are studied with a high performance liquid-crystalline semiconducting polymer, viz. poly(2,5-bis(3-alkylthiophen-2-yl)thieno[3,2-b]thiophene (pBTTT). We present a simple assembly procedure to obtain mixed-type PA-SAMs terminated by methyl and carboxylic acid groups. Tunable surface energy in combination with excellent insulating properties was allowed by this unprecedented mixed monolayer. pBTTT morphology is dramatically affected by the presence of sparse functional groups at the surface. Lithographically defined field-effect transistors operating at low-voltages (<3V) are demonstrated utilizing the mixed-type SAM-based dielectrics. Lower leakage currents, higher on/off ratios, and steeper subthreshold swing are obtained with the mixed-type monolayer, as compared to monolayers fully assembled with carboxylate-containing molecules.

Solution-processable organic semiconductors have attracted substantial interest in recent years due to their processability[1-5], multifunctionality[6-9], and the potential for low-cost fabrication. For polymer semiconductors, performance has been constantly improved, with field-effect mobilities reaching benchmark values of $\geq 1 cm^2V^{-1}s^{-1}$.[10–13] High-performance materials are generally comprised of a rigid π-conjugated polymer backbone functionalized with regularly spaced alkyl side-chains. This molecular design promotes intra/interchain π-π stacking, while allowing the formed crystallites to align parallel to substrates with appropriate surface chemistry. An example for this class of material is the liquid crystalline semiconductor polymer poly(2,5-bis(3-alkylthiophen-2-yl)thieno[3,2-b]thiophene (pBTTT). It shows long-range two-dimensional order,[10] as well as very high field-effect mobilities

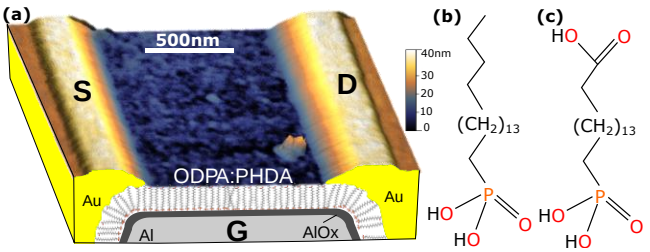

Fig. 1. (a) Schematic representation of the organic transistors with patterned hybrid gate electrodes, prior to spin-coating of pBTTT. A three-dimensional atomic force microscopy image is embedded in the scheme for a device with Al/AlOx functionalized with PHDA:ODPA(1:1). Transistors' source (S), drain (D), and gate (G) electrodes are indicated. The molecular chemical structures are represented in (b) for ODPA, and (c) for PHDA.

(0.1–1 $cm^2V^{-1}s^{-1}$).[14,15] One key step towards the realization of circuitry based on semiconducting polymers is the development of organic field-effect transistors (OFET) operating at low supply voltages, and consequent low power consumption. A very attractive route has been proposed by Klauk *et al.*,[16] wherein they use a hybrid gate dielectric comprised of a thin AlOx and an aliphatic phosphonic-acid (PA) self-assembled monolayer (SAM) to provide high capacitive coupling and low leakage currents. However, due to the very low surface energy obtained with this functionalization, conventional polymer processing methods (e.g. spin-coating) become challenging.[17] To solve this issue, Ball *et al.*[18] have proposed the use of carboxylate-terminated PA-SAMs (16-phosphonohexadecanoic acid, PHDA, Fig. 1) to increase the surface energy, and thus to allow solution processing. However, this has in turn increased the leakage current through Al/AlOx gates. In this communication we show that by functionalizing patterned aluminum gate electrodes with a mixed-type self-assembled monolayer combination – PHDA and octadecylphosphonic acid (ODPA) –, one can simultaneously obtain tunable surface energy while recovering

the insulating performance obtained with highly hydrophobic ODPA-based gate dielectrics. The power of this mixed-SAM approach is demonstrated by fabricating solution-processed OFETs with patterned hybrid gate electrodes by standard lithographic methods. The transistors were tested with pBTTT, whose morphology and electronic properties critically depend on interface chemistry[19] and roughness[20]. Therefore, pBTTT is an ideal candidate to test the quality of these hybrid gate dielectrics.

We present the electronic transport properties of transistors with Al/AlOx gate electrodes functionalized with three different SAM types: (1) PHDA-only, (2) mixed PHDA:OPDA, and (3) mixed PHDA:OPDA with ODPA-only channel. Devices prepared with mixed SAMs show steeper subthreshold swing and over two orders of magnitude lower leakage currents, as compared to the PHDA-only case, whereas full hole mobility is obtained only for the devices with an ODPA-channel. We also studied the impact of the underlying SAMs on the semiconductor morphology by atomic force microscopy (AFM). For ODPA-only monolayers, we observed well-ordered pBTTT terrace-like domains, after annealing above the mesophase transition temperature. This is an interesting result since terraces can only form on very smooth surfaces, while thermally evaporated aluminum (Al) films are generally very rough.

Figure 1(a) shows an exemplary atomic force microscopy (AFM) image of the transistors studied here. An optical microscopy image of the devices can be found in Fig. S04 of the supplementary information. The devices were fabricated with a two-step electron-beam lithography process to define the gate (G), source (S), drain (D), and guard electrodes. Degenerately As-doped silicon wafers with 150nm thermally grown SiO_2 were used as substrates. The gate electrodes were patterned with a PMGI/PMMA double-layer resist combination (process described elsewhere[21]), and with high deposition rates of Al (~10 nm.s^{-1}). The resulting Al patterns (20±3nm thick) were subjected to an oxygen plasma treatment (RIE Oxford Plasma 80Plus, 220mW/cm^2, 20min, 5mbar, 20sccm, 13.56MHz) to produce aluminum oxide (AlOx) of defined thickness, to enhance its quality[22], and to create a high concentration of hydroxyl groups upon air exposure. The samples were then immersed in 1mM solutions of ODPA, PHDA, or a mixture of both, in 2-propanol. Substrates were taken from solution after 1h, rinsed with 2-propanol, and heated to 65ºC for 10min on a hotplate. Low power ultrasonication with 2-propanol removed physisorbed molecules, before the assembly was continued in fresh ODPA solution (healing phase). The surface energy resulting from the assembly of PHDA:ODPA (1:1, for 1h), healed with ODPA, is sufficient to allow spin-coating of PMMA from anisole, without the usual dewetting. Note that samples for leakage current voltage and contact angle measurements were treated in a low-energy plasma system (Diener Pico, 100W, 20min, 20sccm, 2mbar).

Source, drain and guard electrodes were patterned in a second lithography step with the double-layer PMMA resist combination. We deposited 0.3nm of titanium (Ti) by electron-beam evaporation as adhesion layer[23], and 35nm of gold (Au) by thermal evaporation. The resist was stripped in warm acetone, and the sample was rinsed with warm 2-propanol. This carefully optimized process results in hybrid gate dielectrics that routinely show a root-mean-square roughness *Rq*~0.3nm, as shown in Fig. 1(a). The devices were transferred into a nitrogen-filled glove-box (<0.1*ppm* oxygen, <0.1*ppm* water), and thin pBTTT films were cast via spin-coating from warm 0.5%$_{w/w}$ solutions in 1,2-dichlorobenzene. The resulting pBTTT film thickness was ca. 25nm, as measured by stylus profilometry. All transistors had a fixed channel width W of 100µm, and the channel lengths L varied from 40µm down to 0.5µm. A guard electrode was positioned next to the source and drain contacts in order to eliminate fringe currents in the unpatterned semiconducting layer, thus preventing overestimation of mobility and reducing the gate current (I_{gs}). This allows simulating the operation of the transistor as if the pBTTT layer were patterned[24] on top of the gate dielectric. All measurements were performed in vacuum (<2x10^{-4} mbar), after a short exposure to ambient air (<30s).

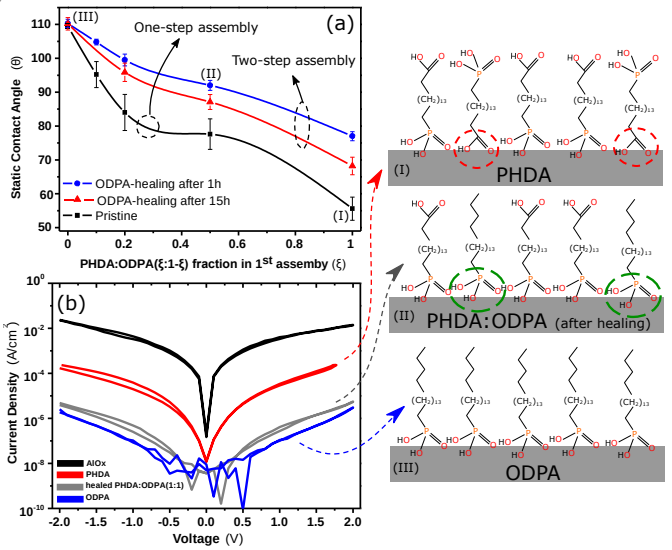

Fig. 2. The healing effect of ODPA on mixed-type SAMs. (a) Static contact angles (SCAs) of water droplets for various fractions of PHDA:ODPA. Black squares: SCAs for one-step assembly. Red triangles: Fully assembled substrates (>15h) healed with ODPA. Blue circles: Incomplete assembly (~1h), healed with ODPA. (b) Current densities for Al/AlOx/PA-SAM/Au junctions and for a Al/AlOx/Au reference junction (black curve). Each case is schematically illustrated on the right.

To evaluate the characteristics of the phosphonic-acid SAM (PA-SAM) type and process method, we performed static contact angle (SCA) measurements (1µL water, 60% air humidity), and two-terminal current-voltage (I-V) measurements. Current densities were analyzed for Al/AlOx/PA-SAM/Au stacks with varied junction areas (1.2–2.5x10^{-4} cm^2). In Fig. 2(a) the SCA is plotted for a range of ODPA:PHDA molar fractions, with the total concentration fixed at 1mM. The *black data points* display SCAs of samples immersed in PA-SAM solution overnight, which indicates higher surface energies for increasing PHDA fractions. SCA values obtained for PHDA-only surfaces are in good qualitative agreement with values obtained previously in the literature[18]. Here, the SCA value of the pristine layer (one-assembly step) was ~10º higher – this small deviation can be expected due to a slight different SAM annealing procedure. Curiously, we found that by re-immersing fully assembled and stabilized monolayers into a solution of pure ODPA, SCA values significantly increased for PHDA-containing monolayers (*red data points*). In a parallel experiment, the first assembly step was set to 1h, which results in incomplete assembly of the PHDA:ODPA(ξ:1-ξ, ξ=0→1) monolayers. For this case (*blue data points*), higher SCA values were observed as compared to monolayers healed after 15h. These observations indicate that loosely bound PHDA molecules can be replaced by ODPA, therefore reducing the overall surface energy. We attribute the loose bonding to surface coordination with the carboxylate terminus, as illustrated in the scheme of Fig. 02 for

PHDA monolayers. The exchange of carboxylate-bound PHDA by ODPA molecules agrees well with a recent study[25], wherein it was shown that molecules with phosphonic acid groups can replace carboxylate-bound molecules on AlOx surfaces.

The outstanding robustness achieved with phosphonic acid-bound SAMs with Al/AlOx gates[26] can be partially attributed to the bonding strength of the phosphonate groups to AlOx surfaces. In turn, weakly (carboxylate-) bound PHDA are expected to have poorer insulating performance. In Fig. 2(b) we show the current densities recorded for a reference AlOx junction (black), PHDA-only (red), PHDA:ODPA(1:1) healed with ODPA (grey), and a junction based on pure ODPA (blue). The increase in current density for PHDA monolayers in comparison to ODPA monolayers is of the same order of magnitude (~10^2) of values reported in the literature[18]. By contrast, for the mixed SAM we observe a remarkable enhancement in insulation, which is imparted by the ODPA healing step. Leakage current reduces by nearly two orders of magnitude, approaching the quality obtained with ODPA-only monolayers. More importantly, lithographic patterned electrodes can be defined since the surface energy is sufficiently high for resist spin-coating. Dewetting of spin-coated PMMA films were only observed for healed mixed SAMs with initial ODPA concentration >50%. Therefore, for all lithographically patterned transistors with mixed SAMs we exclusively used an equimolar mixture of PHDA and ODPA for the first assembly step. Note that the electrical performance of the mixed SAMs was only tested at the later molar ratio. The impact of ODPA content in the mixed PHDA:ODPA SAM leakage current densities has not been directly evaluated.

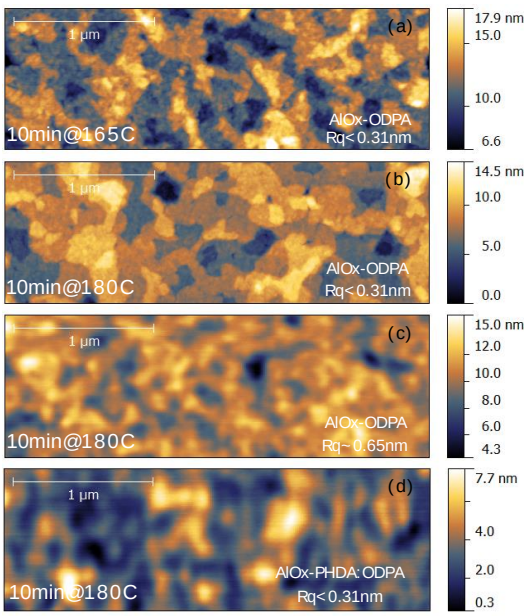

Fig. 3. AFM images of annealed pBTTT on Al/AlOx gates functionalized with ODPA or PHDA:ODPA (1:1, healed with ODPA). The impact of the annealing temperature on smooth ODPA-only channels (Rq<0.31nm) is evaluated for (a) T=165ºC, and (b) T=180ºC. (c) pBTTT on rough ODPA-only channel (Rq~0.65nm) annealed at T=180ºC, and (d) on a smooth channel (Rq<0.31nm) with the mixed SAM annealed at T=180ºC.

Morphological studies of pBTTT thin films have been extensively reported in the literature for various types of substrate surfaces.[27,28] However, to our knowledge, no study has been reported for patterned gate dielectrics based on Al/AlOx/PA-SAM. Molecular terraces of pBTTT are disrupted on rough surfaces (Rq>0.5nm)[20] and/or for surfaces with high surface energy. Obtaining Al surface roughness of Rq<0.5nm generally poses challenges. By controlling the thermal evaporation rate of Al to 8–10nm.s^{-1}, we routinely obtained Rq<0.35nm on substrates maintained at T=320~350K. At these surface roughness levels, pBTTT films on ODPA-terminated gate dielectric show clear terrace-like domains upon annealing above the mesophase transition temperature (~145ºC[29]). Atomic Force Microscopy (AFM) images taken post-lithographically on transistor channels functionalized with ODPA are shown in Fig. 3(a,b,c). Terraced domains of pBTTT (step height 2.1nm) can be easily distinguished for lower roughness channels (Rq<0.31nm, Fig. 3(a,b)), but not on the rougher Al/AlOx/ODPA gates (Rq~0.65nm, Fig. 3(c)). This is in agreement with a similar study on SiO_2/OTS-based dielectrics.[20] Devices annealed at 180ºC display noticeably better-defined terraces, as compared to devices annealed at 165ºC. Annealing at 165ºC for a longer period (30min) improved only slightly the definition of the terraces (Fig. S02 in the supplementary information). An AFM image of pBTTT on ODPA-healed PHDA:OPDA(1:1) is shown in Fig. 3(d). No molecular terracing is observed, even on channels with low surface roughness. This finding emphasizes the importance of the chemical nature of the dielectric surface on pBTTT crystallinity. It has been previously reported that sharp and small pBTTT terraces can form on clean SiO_2 surfaces upon annealing.[19] Surface energies observed for UV-cleaned SiO_2 are usually significantly higher (SCA<10º) than for ODPA-healed PHDA:OPDA(1:1) (SCA=92–94º). Despite this moderate surface energy, the presence of sparse carboxylate groups connected to the flexible alkyl chain (C15), has proven effective in suppressing the reorganization of pBTTT crystallites upon annealing. It thus seems clear that the morphological characteristics of pBTTT on mixed PA-SAMs cannot be explained only in terms of surface energy. We therefore propose that the side chains (C16) of pBTTT intercalate with the underlying mixed-type PA-SAM in the annealing process. Interdigitation of alkyl side chains of polythiophene-based based semiconductors (e.g. poly(3-hexylthiophene-2,5-diyl)) with the alkyl chains of monolayers is known to occur[30]. In this scenario, carboxylate end groups can readily interact with the polymer backbone. In contrast, less reactive and rigid SiO_2 surface cannot interact easily with the pBTTT backbone, given that its C16 side chains protect the semiconducting core.

Figure 4 displays the transfer and output characteristics of pBTTT low-voltage transistors with three types of gate dielectrics. Two devices (Fig. 4(a,b)) were fabricated with mixed-SAM PHDA:ODPA(1:1) healed with ODPA. The third device (Fig. 4(c)) was fabricated with the gate dielectric functionalized with pure PHDA (1:0). One of the mixed-SAM devices was further processed, and had its channel monolayer replaced by pure ODPA (0:1) (Fig. 4(a)). This was done simply by treating the mixed-SAM devices with oxygen plasma and proceeding with the ODPA assembly process. The leakage currents, on-off current ratios $I_{ds}^{on} / I_{ds}^{off}$, and subthreshold swing are significantly improved for devices prepared with the mixed-type SAM, as compared to PHDA-only devices. Leakage currents decreased by a factor of ~10 (evaluated at V_{ds}=−2.5 V and V_G =−3V), whereas I_{ds}^{off} decreased by two orders for the mixed-type SAM.

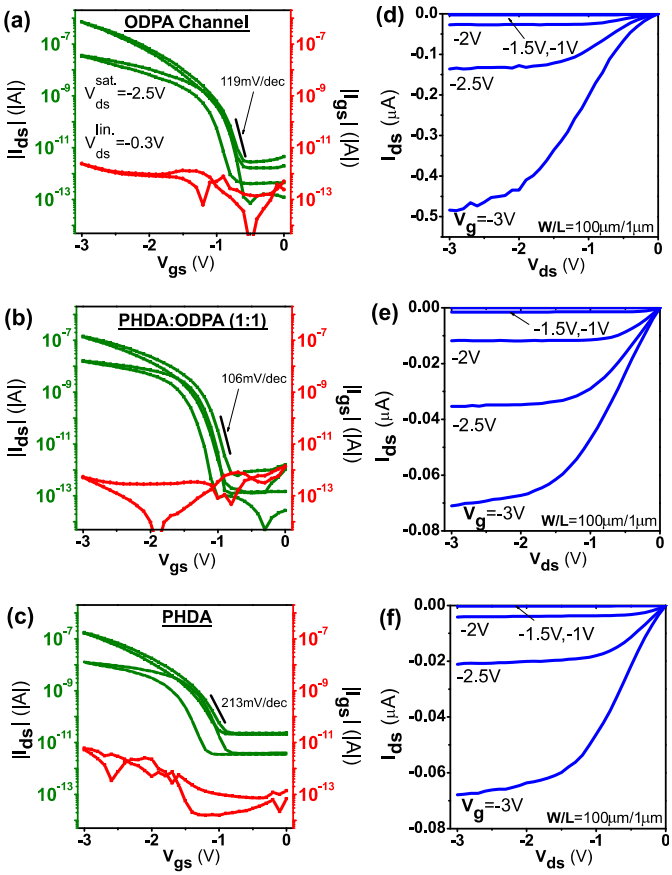

Fig. 4. Electrical properties of lithographically patterned pBTTT transistors. The transfer and output characteristics are depicted for transistors with *W/L* = 100μm/1μm, measured at room temperature and high vacuum. In (a,d) a transistor patterned with PHDA:OPDA(1:1, healed with ODPA) with ODPA-only channel. In (b,e), the transfer and output curves for a PHDA:OPDA(1:1, healed with ODPA) channel. In (c,f), transfer and output curves for a transistor fabricated with PHDA-only monolayer.

Leakage current and I_{ds}^{off} of OFETs with patterned bottom-gate with overlapping bottom-contact geometry (BGBC) are highly sensitive to the thickness and quality of the gate dielectric. Particularly, the I_{ds}^{off} of transistors with very thin hybrid dielectrics can also include spurious contributions from S/D current leaking through the gate electrode. We attribute the observed off-current degradation observed in PHDA-only pBTTT transistors to an increased contribution from spurious gate currents. This result are in contrast to the results reported in Novak *et al.* for PHDA-based OFETs;[31] however, their data has been obtained on devices with a top-contact geometry via shadow-mask patterning. Spurious gate currents in this case are drastically suppressed since the semiconducting layer decouples S/D contacts from the gate dielectric. Moreover, the lithographic patterning of the S/D contacts in our devices comprises of steps (e.g. PMMA baking and solvent removal) that could efficiently remove loosely anchored SAM molecules from the gate dielectric, thereby increasing device's leakage levels. In contrast, for the ODPA-healed PHDA:ODPA(1:1) mixed SAMs, loose-bound carboxylate-anchored PHDA molecules are essentially not present, providing excellent resistance against lithographic processing steps and S/D metal penetration. The mixed-SAM approach can thus reduce I_{ds}^{off}, and consequently increase the I_{ds}^{on}/I_{ds}^{off} ratio of lithographically defined pBTTT OFETs.

The subthreshold swing $S_{s\text{-}th}$ becomes sharper with decreasing PHDA content - $S_{s\text{-}th}$ =213mV/dec (for PHDA-only 1:0), $S_{s\text{-}th}$=106mV/dec (for mixed ODPA-healed PHDA:ODPA 1:1), and $S_{s\text{-}th}$=119mV/dec (for ODPA-only 0:1 channels). This is followed by a variation of the subthreshold voltage – V_{th}= -1.5V (for PHDA-only 1:0), V_{th}= -1.4V (for mixed ODPA-healed PHDA:ODPA 1:1), and V_{th}= -1V (for ODPA-only 0:1). Capacitance per unit area (C_i) values were found to vary for the different types of SAM used: 0.78μF/cm^2 for ODPA-only, 0.8μF/cm^2 for ODPA-healed PHDA:ODPA(1:1), and 0.99μF/cm^2 for PHDA-only (1:0) transistors (Fig. S03 of Supplementary Information). Field-effect mobilities were calculated with their respective capacitance values in the saturation regime (V_{ds}=–2.5V), as shown in Fig. 5. Devices with ODPA-only (0:1) channel had the best performances, with hole mobilities approaching ~0.1cm^{2}V^{-1}s^{-1} for long-channel transistors. On the other hand, PHDA-containing devices exhibit lower field-effect mobilities, irrespective of the carboxylate concentration in the interface. It is interesting to observe that although the reduction of the PHDA fraction improves the overall performance (e.g. on-off current ratios and subthreshold swing), the field-effect mobilities do not improve significantly. We attribute this to the strong disorder in the pBTTT morphology induced by PHDA, as observed by AFM (Fig. 3). Therefore, the formation of long-range order pathways for charge carrier transport is hindered since pBTTT crystallites are pinned at the interface. For PHDA-containing transistors in on-state, the channel resistance dominates the device's series resistance, whereas for devices with ODPA channel the contact resistance has more pronounced impact on the electrical response. This is seen in Fig. 5 as a strong reduction of extrinsic carrier mobility with channel scaling for ODPA-only channel, whereas for PHDA-containing devices the extrinsic mobility is nearly constant.

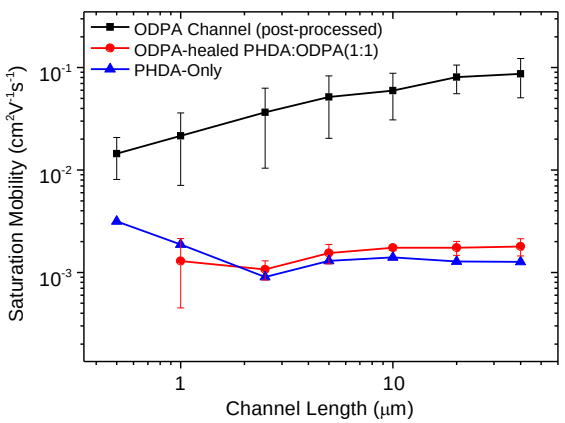

Fig. 5. Extrinsic charge carrier mobility calculated in the saturation regime (μ_{sat}, V_{ds}= –2.5V) after annealing at 165ºC for with fixed channel width (*W* = 100μm) and varying channel lengths. For each surface functionalization type three independent devices with seven junctions each were measured. Error bar plotted for data points with 2 or more working junctions.

Conclusions

In summary, we have shown a simple two-step assembly process for mixed phosphonic acid (PA) monolayers to obtain tunable surface energy, while preserving excellent insulating properties. Our results strongly suggests that the anchoring of PHDA molecules on AlOx

surfaces is not given exclusively via de PA terminal groups, which explain its inferior insulating performance. We combined our method with standard lithography, and fabricated low operation voltage OFETs based on the high performance semicrystalline semiconducting polymer pBTTT. Additionally, we provide a comprehensive study of the morphology of pBTTT on patterned molecular gate electrodes. In particular, we demonstrate that by careful control of the AlOx surface roughness and PA-SAM surface modification, molecular terracing can be observed on pBTTT. The OFET performance was evaluated for three types of channel surface chemistries, namely PHDA, mixed PHDA:ODPA, and ODPA. The overall performance improves for mixed SAMs when compared to PHDA-only devices. Especially for device properties that suffers strong impact from the gate dielectric quality, such as off-state S/D currents and gate leakage. However, mobilities for PHDA-containing devices have significantly reduced in comparison to reference devices with a further ODPA functionalization process step. This detrimental effect has been correlated to high sensitivity of pBTTT morphology to sparse carboxylic acid groups for PHDA-containing SAMs. While this functional group should not act as charge trap sites for hole transporting organic semiconductors, its applicability in n-type devices might be limited to materials with high electron affinity.[32] The proposed method may prove also valuable for the growth of semiconducting oxides via atomic layer deposition, and indeed for any other chemical methods that rely on the presence of functional groups on gate electrode surfaces.

Acknowledgments

This work is supported by the European Union 7*th* Framework Programme (NMP3-SL-2011-263104-HINTS and PIRG06-GA-2009-256470), by the European Research Council (Grant No. 257654-SPINTROS), by the Spanish Ministry of Science and Education (Project No. MAT2009-08494), by the Basque Government (Project No. PI2011-1, PI2010-7, and Etortek Program); and by the Spanish Ministry of Economy and Competitiveness (Project No. MAT2010-16184).

Notes and references

[a] *CIC nanoGUNE Consolider*. Tolosa Hiribidea 76, E-20018 Donostia-San Sebastián, Spain.
[b] *IKERBASQUE - Basque Foundation for Science.* Alameda Urquijo 36-5, E-48011 Bilbao, Spain.

† Electronic Supplementary Information (ESI) available: Atomic Force Microscopy morphological analysis of pBTTT on functionalized, ultrasmooth AlOx prepared via ALD; evaluation of the annealing time on morphological characteristics; gate dielectrics capacitance measurements; optical micrograph of an exemplary device, and further details on materials and experimental Methods. See DOI: 10.1039/c000000x/

1 M. Cavallini, D. Gentili, P. Greco, F. Valle and F. Biscarini, *Nat. Protoc.*, 2012, **7**, 1668–76.
2 A. C. Arias, J. D. MacKenzie, I. McCulloch, J. Rivnay and A. Salleo, *Chem. Rev.*, 2010, **110**, 3–24.
3 J. Rivnay, L. H. Jimison, J. E. Northrup, M. F. Toney, R. Noriega, S. Lu, T. J. Marks, A. Facchetti and A. Salleo, *Nat. Mater.*, 2009, **8**, 952–8.
4 J. Zaumseil, C. L. Donley, J.-S. Kim, R. H. Friend and H. Sirringhaus, *Adv. Mater.*, 2006, **18**, 2708–2712.
5 H. Yan, Z. Chen, Y. Zheng, C. Newman, J. R. Quinn, F. Dötz, M. Kastler and A. Facchetti, *Nature*, 2009, **457**, 679–86.
6 M. Cavallini, P. D'Angelo, V. V. Criado, D. Gentili, A. Shehu, F. Leonardi, S. Milita, F. Liscio and F. Biscarini, *Adv. Mater.*, 2011, **23**, 5091–7.
7 E. Orgiu, N. Crivillers, M. Herder, L. Grubert, M. Pätzel, J. Frisch, E. Pavlica, D. T. Duong, G. Bratina, A. Salleo, N. Koch, S. Hecht and P. Samorì, *Nat. Chem.*, 2012, **4**, 675–9.
8 Y. Ishiguro, R. Hayakawa, T. Chikyow and Y. Wakayama, *J. Mater. Chem. C*, 2013, **1**, 3012.
9 K.-J. Baeg, Y.-Y. Noh, H. Sirringhaus and D.-Y. Kim, *Adv. Funct. Mater.*, 2010, **20**, 224–230.
10 I. McCulloch, M. Heeney, C. Bailey, K. Genevicius, I. Macdonald, M. Shkunov, D. Sparrowe, S. Tierney, R. Wagner, W. Zhang, M. L. Chabinyc, R. J. Kline, M. D. McGehee and M. F. Toney, *Nat. Mater.*, 2006, **5**, 328–33.
11 J. Li, Y. Zhao, H. S. Tan, Y. Guo, C.-A. Di, G. Yu, Y. Liu, M. Lin, S. H. Lim, Y. Zhou, H. Su and B. S. Ong, *Sci. Rep.*, 2012, **2**, 754.
12 W. Zhang, J. Smith, S. E. Watkins, R. Gysel, M. McGehee, A. Salleo, J. Kirkpatrick, S. Ashraf, T. Anthopoulos, M. Heeney and I. McCulloch, *J. Am. Chem. Soc.*, 2010, **132**, 11437–9.
13 X. Zhang, H. Bronstein, A. J. Kronemeijer, J. Smith, Y. Kim, R. J. Kline, L. J. Richter, T. D. Anthopoulos, H. Sirringhaus, K. Song, M. Heeney, W. Zhang, I. McCulloch and D. M. DeLongchamp, *Nat. Commun.*, 2013, **4**, 2238.
14 B. H. Hamadani, D. J. Gundlach, I. McCulloch and M. Heeney, *Appl. Phys. Lett.*, 2007, **91**, 243512.
15 Y. M. Park, J. Daniel, M. Heeney and A. Salleo, *Adv. Mater.*, 2011, **23**, 971–4.
16 H. Klauk, U. Zschieschang, J. Pflaum and M. Halik, *Nature*, 2007, **445**, 745–748.
17 P. H. Wöbkenberg, J. Ball, F. B. Kooistra, J. C. Hummelen, D. M. de Leeuw, D. D. C. Bradley and T. D. Anthopoulos, *Appl. Phys. Lett.*, 2008, **93**, 013303.
18 J. M. Ball, P. H. Wöbkenberg, F. Colléaux, M. Heeney, J. E. Anthony, I. McCulloch, D. D. C. Bradley and T. D. Anthopoulos, *Appl. Phys. Lett.*, 2009, **95**, 103310.
19 R. J. Kline, D. M. DeLongchamp, D. A. Fischer, E. K. Lin, M. Heeney, I. McCulloch and M. F. Toney, *Appl. Phys. Lett.*, 2007, **90**, 062117.
20 Y. Jung, R. J. Kline, D. A. Fischer, E. K. Lin, M. Heeney, I. McCulloch and D. M. DeLongchamp, *Adv. Funct. Mater.*, 2008, **18**, 742–750.
21 T. V. A. G. de Oliveira, M. Gobbi, J. M. Porro, L. E. Hueso and A. M. Bittner, *Nanotechnology*, 2013, **24**, 475201.
22 A. E. T. Kuiper, M. F. Gillies, V. Kottler, G. W. 't Hooft, J. G. M. van Berkum, C. van der Marel, Y. Tamminga and J. H. M. Snijders, *J. Appl. Phys.*, 2001, **89**, 1965.
23 R. T. Weitz, U. Zschieschang, F. Effenberger, H. Klauk, M. Burghard and K. Kern, *Nano Lett.*, 2007, **7**, 22–7.
24 J.-F. Chang and H. Sirringhaus, *Adv. Mater.*, 2009, **21**, 2530–2535.
25 T. Bauer, T. Schmaltz, T. Lenz, M. Halik, B. Meyer and T. Clark, *ACS Appl. Mater. Interfaces*, 2013, **5**, 6073–80.

26 K. Kuribara, H. Wang, N. Uchiyama, K. Fukuda, T. Yokota, U. Zschieschang, C. Jaye, D. Fischer, H. Klauk, T. Yamamoto, K. Takimiya, M. Ikeda, H. Kuwabara, T. Sekitani, Y.-L. Loo and T. Someya, *Nat. Commun.*, 2012, **3**, 723.
27 M. L. Chabinyc, R. Lujan, F. Endicott, M. F. Toney, I. McCulloch and M. Heeney, *Appl. Phys. Lett.*, 2007, **90**, 233508.
28 F. M. Li, P. Dhagat, H. M. Haverinen, I. McCulloch, M. Heeney, G. E. Jabbour and A. Nathan, *Appl. Phys. Lett.*, 2008, **93**, 073305.
29 S. Bain, PhD Thesis, University of Southampton, 2011.
30 D. H. Kim, Y. D. Park, Y. Jang, H. Yang, Y. H. Kim, J. I. Han, D. G. Moon, S. Park, T. Chang, C. Chang, M. Joo, C. Y. Ryu and K. Cho, *Adv. Funct. Mater.*, 2005, **15**, 77–82.
31 M. Novak, T. Schmaltz, H. Faber and M. Halik, *Appl. Phys. Lett.*, 2011, **98**, 093302.
32 L.-L. Chua, J. Zaumseil, J.-F. Chang, E. C.-W. Ou, P. K.-H. Ho, H. Sirringhaus and R. H. Friend, *Nature*, 2005, **434**, 194–9.

TABLE OF CONTENTS

Highly insulating gate dielectrics based on AlOx and on mixed phosphonic-acid SAM terminated with methyl/carboxylic acid groups are demonstrated.